

Stars and Dark Matter in the Spiral Gravitational Lens 2237+ 0305

C. M. Trott^{1?}, T. Treu^{2,4}, L. V. E. Koopmans³ and R. L. Webster¹

¹School of Physics, University of Melbourne, Victoria 3010, Australia

²Department of Physics, University of California, Santa Barbara, CA 93106, USA

³Kapteyn Astronomical Institute, P.O. Box 800, 9700 AV Groningen, The Netherlands

⁴Sloan Fellow, Packard Fellow.

21 February 2024

ABSTRACT

We construct a mass model for the spiral lens galaxy 2237+ 0305, at redshift $z_1=0.04$, based on gravitational-lensing constraints, HI rotation, and new stellar-kinematic information, based on data taken with the ESI spectrograph on the 10m Keck-II Telescope. High resolution rotation curves and velocity dispersion profiles along two perpendicular directions, close to the major and minor axes of the lens galaxy, were obtained by fitting the Mg-Fe absorption line region. The stellar rotation curve rises slowly and flattens at $r \approx 1.5^{+0.0}_{-0.1}$ (1.1 kpc). The velocity dispersion profile is approximately flat. A combination of photometric, kinematic and lensing information is used to construct a mass model for the four major mass components of the system – the dark matter halo, disc, bulge, and bar. The best-fitting solution has a dark matter halo with a logarithmic inner density slope of $\gamma = 0.9 \pm 0.3$ for ρ_{DM} / r , a bulge with $M/L_B = 6.6 \pm 0.3$, and a disc with $M/L_B = 1.2 \pm 0.3$, in agreement with measurements of late-type spirals. The bulge dominates support in the inner regions where the multiple images are located and is therefore tightly constrained by the observations. The disc is sub-maximal and contributes 45 \pm 11 per cent of the rotational support of the galaxy at $2.2r_d$. The halo mass is $(2.0 \pm 0.6) \times 10^{12} M_\odot$, and the stellar to virial mass ratio is 7.0 ± 2.3 per cent, consistent with typical galaxies of the same mass.

Key words: dark matter | galaxies: kinematics and dynamics | galaxies: structure
| galaxies: individual (2237+ 0305)

1 INTRODUCTION

Strong gravitational lensing has been used extensively to model galactic- and cluster-mass systems (e.g. Maller et al. 2000; Trott & Webster 2002; Winn et al. 2003; Sand et al. 2004; Bradac et al. 2006; Halkola et al. 2006; Yoo et al. 2006; Jiang & Kochanek 2007; Limousin et al. 2007; Bolton et al. 2008; Grillo et al. 2008). The combination of lensing information with photometric and kinematic data can be used to break degeneracies inherent to each source of information (e.g. the mass-sheet degeneracy and the mass-profile anisotropy degeneracy) to produce a well-constrained mass model for the system (e.g. Koopmans et al. 1998; Winn et al. 2003; Koopmans & Treu 2003; Treu & Koopmans 2004; Czoske et al. 2008; Koopmans et al. 2006). This is particularly important

in spiral galaxies which have multiple mass components that have to be modelled simultaneously, and the limitations of individual methods are particularly stringent. Specifically, in the absence of kinematic information, lens image positions can accurately constrain the enclosed mass, and to some extent also constrain the mass distribution up to a constant mass-sheet (Gorenstein et al. 1988; Wambsganss & Paczynski 1994; Wucknitz 2002). When assuming a stellar mass-to-light ratio for the different optical components (e.g. disc and bulge), based, for example, on stellar-population synthesis models, the dark matter contribution to the galaxy can then be inferred. In the absence of lensing information, but with kinematic data in hand, the overall galactic mass distribution is known, but again a stellar mass-to-light ratio must be assumed for the optical components in order to infer the contribution of the dark matter (the disc-halo degeneracy, Perez et al. 2004; Verheijen et al. 2007). Because of the rising contribution

? Email: ctrott@pet.mgh.harvard.edu

of the stellar mass components, this becomes increasingly more difficult towards the inner regions of the galaxy. With the combination of lensing and high-resolution kinematic information, however, the stellar mass-to-light ratios of the optical components can be further constrained, breaking some of the degeneracies between mass, mass-slope and anisotropy (e.g. Trott & Webster 2002; Treu & Koopmans 2004, and references therein).

An accurate model for the mass distribution in spiral galaxies can provide interesting information about both the baryonic and the non-baryonic components. Disentangling these components provides information about the mass-to-light ratios as well as the influence, shape and density profile of the dark matter. The main motivations of this work are to: (1) break the classical degeneracy between the stellar component and the dark-matter halo in spiral galaxies (van Albada & Sancisi 1986), using the additional information that lensing provides; (2) determine independent mass-to-light ratios for the bulge and disc components; (3) determine whether the disc component is ‘maximal’ (e.g. Sackett 1997; Courteau & Rix 1999). In more general terms, understanding the relative mass of the different components can help constrain models for disc galaxy formation (e.g. Dutton et al. 2005, 2007, and references therein, see also Shin & Evans (2007)). In addition, the presence of massive discs in spiral galaxies gives rise to interesting perturbations to the standard elliptical models adopted for early-type galaxies with a number of interesting consequences for the topology of the time delay surface (Moller et al. 2003).

In this paper, we address these issues by studying the gravitational lens galaxy 2237+ 0305. Newly measured rotation curves and line-of-sight velocity dispersion profiles along two directions close to the major and minor axes (obtained from Keck-ESI spectroscopy) are combined with photometric and lensing data from HST to construct a detailed mass model for the system. This is used to separate luminous and dark matter over scales ranging from the central parts dominated by the bulge out to several exponential scale lengths of the disc component, with the aid of HI data.

The lens system 2237+ 0305 (chosen for this study due to the low redshift of the lens galaxy $z_l = 0.04$) has been observed extensively since its discovery in 1985 (Huchra et al. 1985). In addition to providing information about the global mass structure of the galaxy (Schneider et al. 1988; Kent & Falco 1988; Mihov 2001; Trott & Webster 2002), it has also been used to study the properties of stars, or compact objects, in the lensing galaxy through microlensing (e.g. Gilmerino & Lewis 2005), and the structure of the broad-line region of the lensed quasar (Wyth et al. 2005; Vakulik et al. 2007; Eigenbrod et al. 2008b). Previously published spectra of 2237+ 0305 have either concentrated on studying the quasar spectrum, or only presented a small wavelength range for the galaxy spectrum. The discovery paper, Huchra et al. (1985), presented a quasar spectrum taken with the MMT and featured both the C IV and C III] broad lines. In addition, they identified the H + K break at 4100 Å and Mg b absorption (5381 Å). This spectrum was not of sufficient quality to identify any further features, but was successful in its primary aim: to confirm the system as a lens. Foltz et al. (1992) observed the galaxy to determine a velocity dispersion for the bulge. They identified Mg b and Fe I absorption features, but also only presented a spectrum

over a small wavelength range (5100–5550 Å). Lewis et al. (1998) concentrated their observations around the quasar emission lines to investigate variations between the four images, thereby inferring microlensing effects (line and continuum regions are expected to behave differently under microlensing conditions because the flux emanates from regions of different source size). The system 2237+ 0305 has also been the subject of several microlensing monitoring experiments to study the size of the quasar emitting regions (Wozniak et al. 2000; Udalski et al. 2006; Eigenbrod et al. 2008a). Rauch et al. (2002) identified absorption lines in the spectrum from intervening (between lens and source) objects using the HIRES spectrograph on Keck. These spectra display high-resolution absorption line profiles of the intervening systems and as such do not concentrate on the spectrum of the galaxy as a whole.

van de Ven et al. (2008) have recently obtained GMOS IFU data of the Ca II near-infrared triplet from the central region of 2237+ 0305 to determine the contribution of dark matter in the central regions of the galaxy. They demonstrated that within the central projected $4''$, dark matter can contribute no more than 20% of dynamical mass, using single stellar population models to constrain the stellar mass contribution, and both lensing and inferred kinematics to constrain the total dynamical mass. Our results agree with those of van de Ven et al. (2008) in the region of overlap. However, our methodology and aims are significantly different, as our goal is to construct a simply parametrized model to describe the data over a tenfold radial extent.

In a previous analysis of the system, Trott & Webster (2002) combined lensing and photometric data to constrain the inner mass distribution of the galaxy. In addition, neutral hydrogen rotation points at large radius were used to study the influence of the outer dark matter halo. They found that additional kinematic information was required in the image region to break the remaining model degeneracies. Specifically, the inner logarithmic slope of the dark matter halo, a contentious issue (see for example Hayashi et al. 2004; de Blok 2005), could not be constrained without additional information about the inner regions of the galaxy.

In contrast, this paper presents mass-to-light ratios for the bulge and disc components that do not require stellar population-synthesis models to constrain the stellar M/L ratios, and are therefore independent measurements. The only assumption is that the mass-to-light ratio is constant across the component. This also allows us to quantitatively assess the contribution and density profile of the inner dark-matter halo in this high-mass spiral galaxy, complementing work done in dwarf and low surface brightness spiral galaxies (de Blok et al. 2001; Borriello & Salucci 2001; de Blok 2005; Zackrisson et al. 2006). Furthermore, whereas in Trott & Webster (2002) the halo was constrained to have a softened isothermal shape due to the absence of kinematic data, in this paper we have allowed for a more flexible model.

The paper is organized as follows. Section 2 describes spectroscopic observations of 2237+ 0305 with ESI on Keck, presents the resulting optical spectrum and uses absorption features to derive both an optical rotation curve and line-of-sight velocity dispersion profile along perpendicular axes. Section 3 introduces the modelling: Section 3.1 describes the mass density models used for each component; a two-integral axisymmetric model of the galaxy that is used to generate

Date	PA	Slit Position	Slit Width	Exposure
		$^{\circ}$	$''$	Seconds
2001 July 21	65	5 (offset)	1.25	1200
2001 July 21	155	5 (offset)	1.25	1200
2001 July 21	155	centred	1.25	1200
2001 July 23	65	centred	1.25	1800

Table 1. Observing log.

the observed kinematics is introduced in Section 3.2; then Section 3.3 describes the algorithm used to find the solution. Sections 4 and 5 present the results of the modelling and some discussion, and Section 6 concludes. We assume $m = 0.3$, $\alpha = 0.7$ and $H_0 = 70 \text{ km s}^{-1} \text{ Mpc}^{-1}$ throughout this paper.

2 SPECTROSCOPY AND STELLAR KINEMATICS

In this Section, the Echelle Spectrograph and Imager (ESI) on the Keck-II telescope is used to measure a high spectral and spatial resolution spectrum of the galaxy 2237+0305 and the lensed quasar images. The spectra are used to extract a rotation curve and velocity dispersion profile for the galaxy, based upon measurements of the Mg b absorption line. The results are consistent with measurements (van de Ven et al. 2008) in the region of overlap but extend them considerably in extent.

2.1 Observations

The lens galaxy 2237+0305 was observed as part of the Structure and Dynamics Survey (LSD, e.g. Koopmans & Treu 2002), a project that aims to obtain stellar kinematic information in lens galaxies to improve modelling and break degeneracies in their mass models. The data were taken on 2001 July 21 and 23 with the Keck II telescope on Mauna Kea, Hawaii. Conditions were clear and the seeing was $0.9''$. The Echelle Spectrograph and Imager (ESI) instrument was used in echelle mode, providing a constant pixel size of $11.9 \text{ km s}^{-1} \text{ pixel}^{-1}$ across all orders, and a spatial resolution along the slit of approximately $0.154 \text{ arcsec/pixel}$ (depending on the order). The galaxy was observed with a $1.25''$ slit width giving a kinematic resolution of $\Delta v = 36.1 \text{ km s}^{-1}$.

The target was observed along two perpendicular slit directions, sampling close to the lens galaxy major and minor axes and trying to avoid the locations of the lensed quasar images. Table 1 summarises the key observational data for the galaxy. Note that the major axis is at a position angle of 77° (measured as usual East from North). Although the observations were taken at $12''$ from the major and minor axes to minimise quasar contamination, for simplicity the two slit angles will be referred to as the ‘major’ and ‘minor’ axes herein. The misalignments are taken into account in the modelling. Two of the spectra were observed with the galaxy offset $5''$ from the slit centre in order to sample the outer regions on one side.

In addition to the galactic exposures, template stellar

spectra are required to measure the rotation and velocity dispersion of the galactic spectral features. The bulge of the galaxy is primarily observed in these observations, and so template spectra are needed of old red stars expected in such an environment. The I-band images of 2237+0305 presented in Yee (1988) show the central $12''$ to be dominated by old and red stars with $\langle g-r \rangle = 0.58$ ($\langle V-R \rangle = 0.9$, Windhorst et al. 1991) consistent with Giant K 0 III (K 5 III) stars. A set of appropriate stellar templates, described by Sand et al. (2004), were observed during the same run and are used in this analysis.

2.2 Optical spectrum and lens galaxy kinematics

Data reduction was performed using the EASI2D software package, developed by David J. Sand and T. Treu (Sand et al. 2004). Details of the data reduction are given in Appendix A.

Figure 1 displays the first eight of the ten spectral orders (the remaining two orders do not show any relevant features of the lens galaxy) obtained by averaging the central four arcseconds in order to increase the signal-to-noise ratio. Four arcseconds correspond approximately to the region over which $S/N > 5$ per unbinned spatial pixel. A relative flux calibration was performed. Prominent spectral features are marked on the spectra. The line-of-sight absorption systems reported in Rauch et al. (2002), between the lens galaxy and background quasar, are also confirmed in these spectra ($z = 0.5656$: Mg I 4486Å, Mg II 4377Å, Fe II 4070Å; $z = 0.827$: Mg II 5108Å, Fe II 4867Å). There are no obvious galactic emission lines at the redshift of the lens, as expected from an old stellar population. The H α absorption line (6821Å observed) is partly obscured by the B-band atmospheric water vapour absorption line in lower resolution spectra, however our higher resolution observations can separate the two lines and H α emission is not found to be present. The broad emission lines of the lensed quasar images, C IV (4175Å), C III] (5145Å) and Mg II (7541Å) are prominent, with C IV and Mg II suffering from sky absorption (see also Huchra et al. 1985).

The spectra were used to measure the rotation curve and line-of-sight velocity dispersion profile for the major and minor axes as described in Appendix A. Figure 2 displays the best fits and their uncertainties. The major-axis velocity dispersion profile is relatively flat, immediately suggesting an underlying isothermal density profile (e.g. Bertin et al. 2002).

3 THE GALAXY MODEL

In Trott & Webster (2002), it was argued that kinematic information could break the remaining degeneracies (see discussions above) between models. No kinematic information for the galaxy centre was available at that time, however, and degeneracies remained in the modelling. With new high quality kinematic information in hand, we can now further constrain the mass distribution.

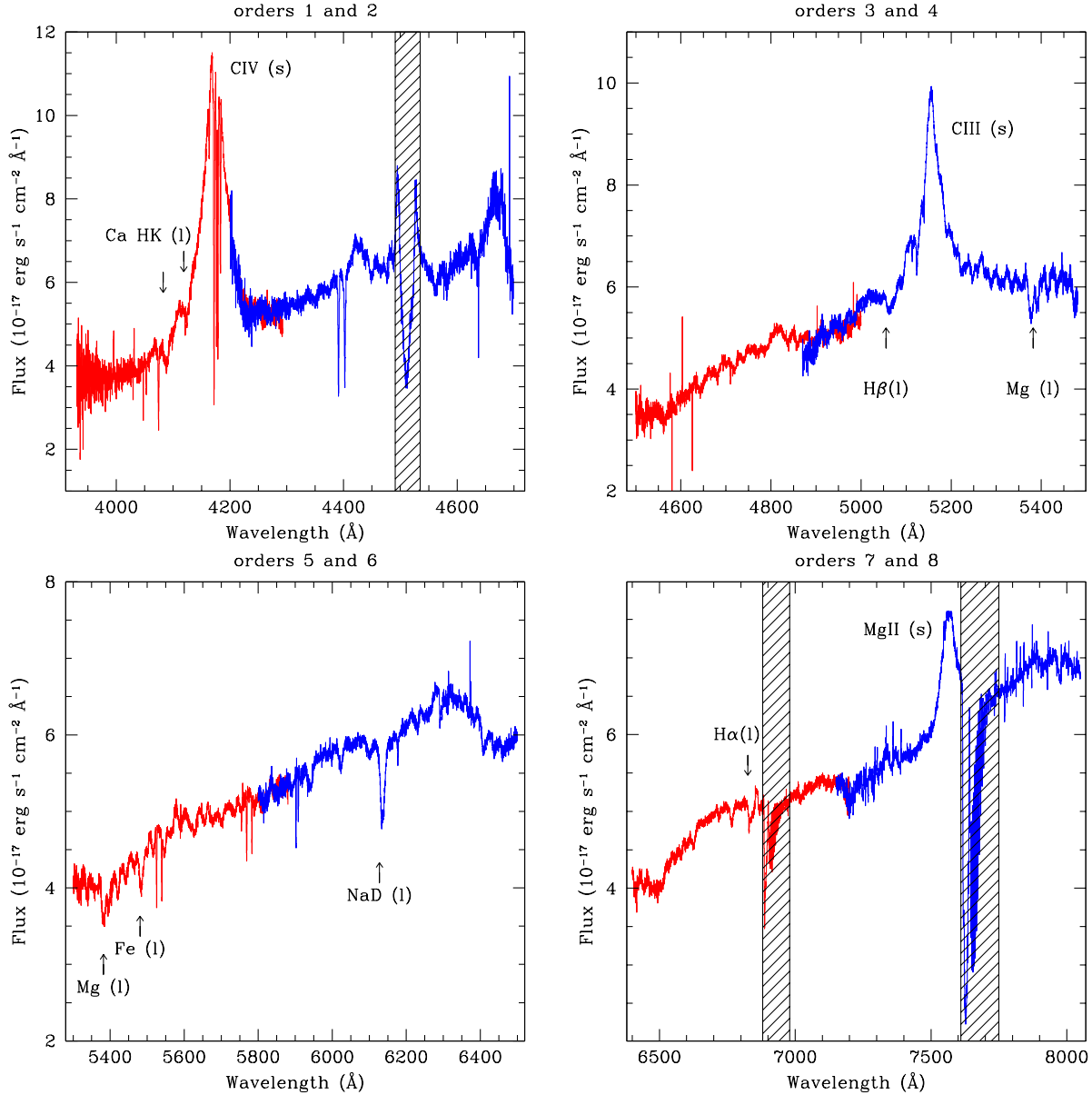


Figure 1. Sky-subtracted spectra of 2237+0305 taken at a position angle 12° clockwise from that of the major axis. The spectra have been flux calibrated up to a constant factor based on ESI standard response curve, measured in July 2001. Two orders are shown in each plot (odd and even orders in red and blue respectively). Relevant features are labelled for the lensed source (s) and for the lens galaxy (l). A set of bad columns in order 2 and the atmospheric A and B band in orders 7 and 8 are indicated by shaded regions.

3.1 Mass models

Given the larger number of constraints with the addition of kinematic information, one can accommodate more flexible models for the mass components than Trott & Webster (2002). There is no reason to change the modelling of the disc (exponential surface density) and bar (Ferrers ellipse – although the non-axisymmetric component of the bar will not be considered for the inner kinematic model), since these are based on visible light profiles. For the kinematic analysis, the exponential disc is deprojected to an exponential term for the z -direction (Binney & Tremaine 1987). The distribution of dark matter remains unknown, and a more general profile can be fitted than was used in Trott & Webster (2002).

3.1.1 Stellar component

For tractability, we assume a model for the bulge component that is simple and retains the key features that are required both for the lensing and kinematic constraints. In previous work, and following that of Schmidt (1996), the bulge is modelled by a flattened de Vaucouleurs surface brightness profile. The latter is one of a class of Sersic profiles (Sersic 1968):

$$I(R) = I_0 \exp \left[-b_n \left(R/r_b \right)^{1+m} \right]; \quad (1)$$

r_b is the characteristic scale length and b_n is a constant. A de Vaucouleurs profile corresponds to $m = 4$, with an appropriately scaled r_b .

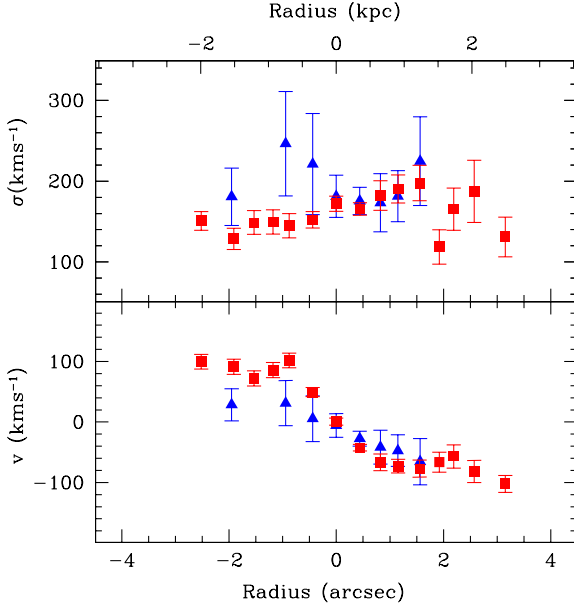


Figure 2. Velocity dispersion profile and rotation curve for the major (red squares) and minor (blue triangles) axes. The larger error bars far from the galactic centre reflect the lower signal-to-noise in these regions.

Lin & Neto et al. (1999) and Lokas et al. (2005) present de-projections of the circularly symmetric Sersic profile, which allow one to use kinematic expressions for the rotation speed and line-of-sight velocity dispersion. We generalise these for a non-spherical density profile, because a flattened bulge component is important for the lensing. The deprojected elliptical Sersic profile for general m is given by,

$$\rho(r) = \rho_0 \exp\left(-\frac{r}{r_h}\right)^{1+m}; \quad (2)$$

$$\rho_0 = \frac{(2m)}{2} \frac{\rho_b}{[(3-p)m]}; \quad (3)$$

$$p = 1.0 - 0.6097m + 0.05463m^2; \quad (4)$$

$$r_h = (r_b)^m \quad (5)$$

where r_h is a generalised scale length, ρ_0 is the central surface mass density ($\rho_0 = \rho_b$ for connection with the lensing, and ρ_{cr} is the critical surface mass density), and $r^2 = r^2 + z^2 b^2 = a^2$ is the elliptical radius, where a and b are the semi-major and -minor axes. We use the expressions of Noodin et al. (2008) to describe the rotation curve of an elliptical Sersic profile.

The scale length and ellipticity of the bulge were measured from a two-dimensional fit of the HST NICMOS image (Proposal ID: 7495, PI: Falco). After simulating the NICMOS point spread function with TINYTIM (Hasan & Burrows 1995), a Sersic plus point source (quasars) model was fitted with the *gal* software (Peng et al. 2002), yielding a Sersic index of $m = 4.0 \pm 0.1$, a scale length of $r_b = 4.07 \pm 0.10''$ and a projected axis ratio of $(a/b)_{b,pr} = 0.64 \pm 0.01$. We use an intrinsic axis ratio of $(a/b)_{b,in} = 0.6$ (van de Ven et al. 2008).

3.1.2 Dark matter component

The dark matter halo is modelled with a spherical generalised cusp, with variable inner and outer density slope (Zhao 1996; Muñoz et al. 2001; Keeton 2001). This profile reduces to a variety of useful models, such as the NFW, Hernquist and isothermal, and has the form,

$$\rho(r) = \frac{s}{(r=r_h) [1 + (r=r_h)^2]^{(n+2)/2}}; \quad (6)$$

where s and n are the inner and outer logarithmic slopes, respectively, and r_h is the characteristic scale length. For a spherical model, the lensing convergence, κ , is given by,

$$\kappa(x) = \frac{n}{2} \frac{1}{x^2} {}_2F_1\left(\frac{n}{2}; \frac{n}{2}; \frac{1}{1+x^2}\right); \quad (7)$$

where $x = r/r_h$, $B(\cdot, \cdot)$ is the beta function and ${}_2F_1(\cdot, \cdot)$ is a hypergeometric function (Buchholz 1969). In our model, the outer logarithmic slope, n , will not be well constrained as most of the constraints lie within $5''$ of the galaxy centre. It is set to a value of 3, consistent with N-body simulations (Navarro et al. 1996; Moore et al. 1999; Navarro et al. 2004).

3.2 Kinematic modelling

To model the lensing and kinematic data-sets of 2237+0305, we assume that the central regions of the galaxy can be well approximated by an axisymmetric two-integral distribution.

We solve the two-integral Jean's equations from which we obtain the velocity dispersion profile and mean streaming motion of the galaxy. We follow the prescription of van der Marel & van Dokkum (2007), details of which are described in Appendix B, and solve the two-integral axisymmetric Jean's equations on a grid. We model the bulge+bar as one single axisymmetric component, ignoring the second-order non-axisymmetric bar component.

Jean's equations provide the first two dynamical moments,

$$\overline{v_w^2}(x; y) = \frac{1}{(x; y)} \int_0^{\infty} (x; y; w) \overline{v_w^2}(x; y; w) dw; \quad (8)$$

where w denotes the line-of-sight direction and

$$\overline{v_w^2} = \overline{v^2} \cos^2 i; \quad (9)$$

are the first and second moments, i is the inclination angle, and R and ϕ are the radial and azimuthal directions. The rotation component, V , and velocity dispersion, σ , are then derived as,

$$V = \langle \overline{v_w} \rangle; \quad (10)$$

$$\sigma^2 = \overline{v^2} - \frac{V^2}{\cos^2 i} = \overline{v^2} - \frac{V^2}{\cos^2 i}; \quad (11)$$

The effects of seeing, pixel size and slit width are incorporated into the modelling using the Monte-Carlo technique of van der Marel (1994). The luminosity-weighted moments are convolved with the point spread functions that characterise the slit width, pixel size and seeing. This is accomplished by randomly sampling the region of the galaxy

Component	Parameter	Value	Definition
Bulge	b	free	convergence
	r_b	4.07^{00}	scale length
	$a=b_{\text{proj}}$	0.64	projected axis ratio
Rotation	k	free	rotational support
Disc	d	free	convergence
	r_d	11.3^{00}	scale length
	$a=b_d$	0.5	axis ratio
DM Halo	h	free	convergence
	r_h	free	scale length
		free	inner slope
	n	3.0	outer slope
Bar	br	free	convergence
Source	x	free	x source position
	y	free	y source position

Table 2. Parameters to be fitted in the combined lensing and kinematic model of 2237+0305. The ellipticities of the bulge and disc are fixed at their photometric value, and the bar and disc scale lengths are modelled as in Schmidt (1996) with only a variable M/L . There are 9 parameters in total.

in question and averaging luminosity-weighted samples: a point is chosen randomly (uniform sampling) from within the slit and pixel, and then a normal deviate (with FWHM equal to the seeing) is added. The kinematics at this point are computed and added (with a weight proportional to the galaxy luminosity at that point) to previous samples. This method produces good results without having to perform expensive numerical convolutions. We sample 3000 points for each datum to arrive at our observed moments. By computing kinematics with a larger number of samples and comparing output, we find that 3000 samples are sufficient to produce accurate results (error < 10% of measurement error).

3.3 Mass model optimization

The algorithm for consistently solving for the kinematics and lensing constraints involves a simplex minimisation of the χ^2 of the mass model. Specifically, we: (1) construct a galaxy mass model as described in Section 3.1 with parameters shown in Table 2; (2) calculate the lens image positions based on this model; (3) calculate the observed rotation and velocity dispersion profile based on a summation of the disc, bulge and dark matter halo components; (4) calculate the expected rotation at the location of the outer H I measurements from all mass components; (5) compute a χ^2 for the model as a summation of the adequacy of fits for the lens positions, inner kinematics and outer kinematics; (6) iteratively change the parameters until an acceptable minimum is obtained.

The parameters in the model are given in Table 2, including the unknown source position. We use the HST-derived image positions of Crane et al. (1991), as in Trott & Webster (2002).

The constraints¹ include the four image positions, the

Component	Parameter	Value
Bulge	$M=L_B$	6.6 ± 0.3
	b	103 ± 5
	r_b	4.07^{00}
	k	1.0 ± 0.1
Disc	$M=L_B$	1.2 ± 0.3
	d	0.014 ± 0.004
	r_d	11.3^{00}
DM Halo	h	0.010 ± 0.003
	r_h	$(31.7^{+15.0}_{-9.0})^{00}$
		0.9 ± 0.3
	n	3.0
Bar	br	0.06 ± 0.01
Source	E	-0.058 ± 0.006^{00}
	N	-0.015 ± 0.006^{00}
Magnification	Image A	4.3
	Image B	4.4
	Image C	-2.4
	Image D	-5.1
	tot	16.2
χ^2_{reduced}		2.2

Table 3. Parameter values for the best-fitting solution with reduced $\chi^2 = 2.2$. Here, E and N refer to the source position relative to the galactic centre. Uncertainties are also shown corresponding to an increase of one in the χ^2 , while marginalising over the remaining parameters.

two H I rotation points and the kinematic information, with points in the minor axis rotation curve removed due to contamination, giving 54 constraints, and 45 degrees of freedom.

The χ^2 statistic quantifying the goodness-of-fit for a model is defined as,

$$\chi^2 = \sum_{\text{Images}} \frac{(\text{model})^2}{2} + \sum_{r_{HI}} \frac{(v - v_{\text{mod}})^2}{v^2} \quad (12)$$

$$+ \sum_{r_{\text{Keck}}} \frac{(v - v_{\text{mod}})^2}{2 v_{\text{data}}} + \sum_{r_{\text{Keck}}} \frac{(\text{data} - \text{model})^2}{2 \text{data}};$$

where the summations are over lens image positions, H I rotation points, Keck major and minor axis rotational values and Keck major and minor axis velocity dispersion values, respectively. The reduced χ^2 , given the large number of degrees of freedom, is defined as $\chi^2/45$. A reduced χ^2 of unity is a statistically acceptable fit. Image position errors are 8 mas, consistent with measurement errors.

4 RESULTS

Table 3 lists the parameters for the best-fitting model and the 1 σ uncertainties for each parameter, defined as the parameter value corresponding to an increase in the χ^2 of one while marginalising over the other parameters. This is

added complexities of modelling microlensing, substructure and the effects of differential dust extinction, however we do calculate the resultant ratios and compare them with mid-IR measurements as a model sanity check.

¹ Flux ratios were not used to constrain the models due to the

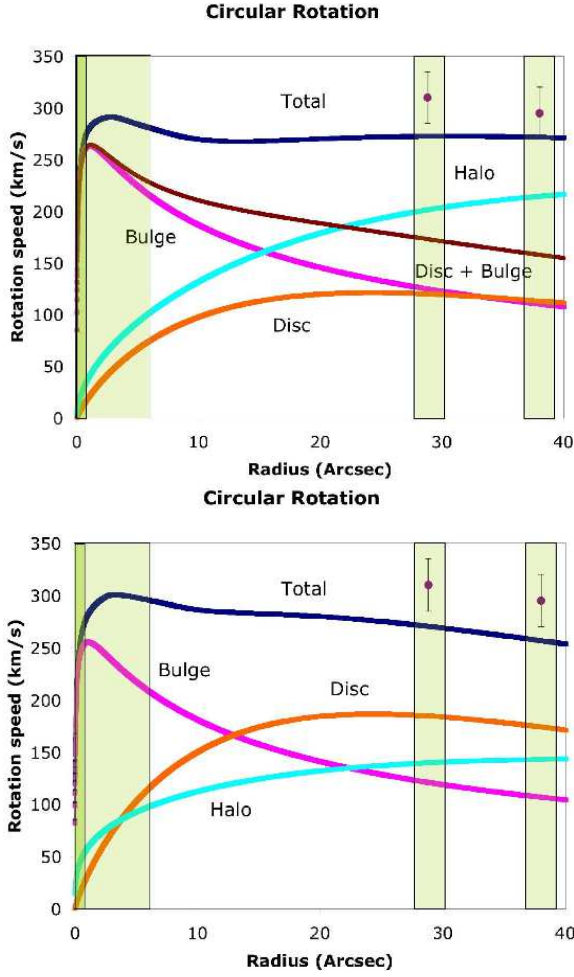


Figure 3. (Upper) Rotation curve (edge-on) for the solution with the best χ^2 . Light-shaded regions indicate radii where kinematic information is available. The dark-shaded region in the galactic centre indicates where the lensing information is useful. The two HI points are shown with their 1σ measurement uncertainties. The contribution of the luminous component alone (disc+bulge) is also displayed. (Lower) Rotation curve for a solution with minimum dark matter halo. This solution is allowed within the 3σ error bars and demonstrates the disc-halo degeneracy in the model.

achieved by sampling select points in parameter space, and determining where the χ^2 increased by one. Specifically, to determine the uncertainty on parameter, α , for example, we performed a full minimization for several values of α (i.e., set the value of α and allow all other parameters to vary to find the minimum) and find the value for α where the χ^2 value increased by one from the global minimum.

Figure 3 (upper) displays the circular velocity curve for the best model. Also displayed are regions of the galaxy where kinematic or lensing information adds constraints. As expected, the model with the best-fitting solution is bulge-dominated in the central regions and has a stellar disc that, combined with the bulge, supports the majority of the rotation to $r \approx 20''$, beyond which the dark matter halo dominates. The inner dark matter halo slope is consistent both with an NFW profile and a central core at $3''$. The bulge

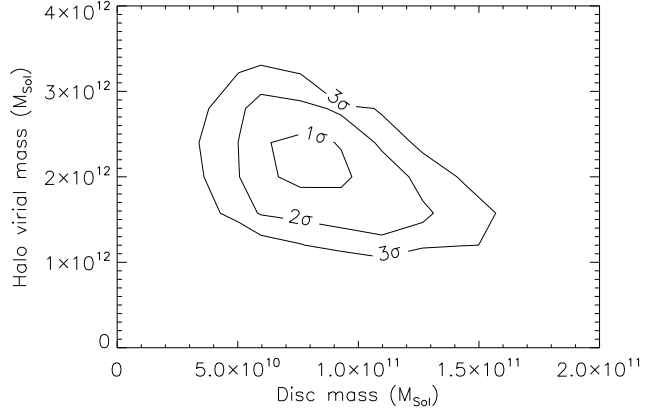


Figure 4. Degeneracy between the disc mass and halo virial mass, with contours at 1, 2 and 3 above the minimum ($\chi^2_{\min} + 2.3, 6.2, 9.2$).

and disc mass-to-light ratios are consistent with previous measurements. Table 3 also displays the image magnifications and total magnification for the model. The flux ratios are consistent with the mid-IR measurements of Agol et al. (2000), providing a good sanity check for the model.

Figure 3 (lower) displays the rotation curve of a solution that is at the very edge of what is allowed by the uncertainties (3σ), having a minimum dark matter halo and a more prominent disc. The relatively large errors on the HI data points, the freedom of the dark matter model and the lack of kinematic information between 5 and 30 arcseconds, combine to allow at 1σ level a low-mass halo model. This demonstrates that the familiar disc-halo degeneracy, where the disc convergence and shear can account for the halo contribution, is almost completely broken. Figure 4 demonstrates the degree of degeneracy between the disc mass and halo virial mass. As expected, these parameters are correlated, but the system does not allow a large range for either. In a system with a larger disc-halo degeneracy, the range of disc and halo κ values would be increased. In 2237+0305, the bulge contributes the majority of the lensing convergence and shear, with the disc and bar both also contributing convergence and shear, and the halo contributing convergence alone (spherical model). Although the bulge cannot change to account for the disc shear, there is freedom in the bar model to account for this. As such, 2237+0305 is a good system to break the disc-halo degeneracy. Even tighter constraints can be obtained in the future if kinematic information is available at a larger range of radii (notice that the shape of the total rotation curve is different between the two figures). Future studies, including a prior on the stellar mass-to-light ratio of the bulge and improved kinematic data, should be able to further limit the remaining degeneracy between the halo and disc mass.

We emphasize, however, that there are correlations between other modelled parameters. The bulge, being the dominant component for the lensing, is well-constrained and displays only mild correlations with both the disc and halo κ (results not shown), supporting our assertion that the disc-halo degeneracy is the most prominent. In terms of halo parameters, the halo convergence (κ_h) and inner slope

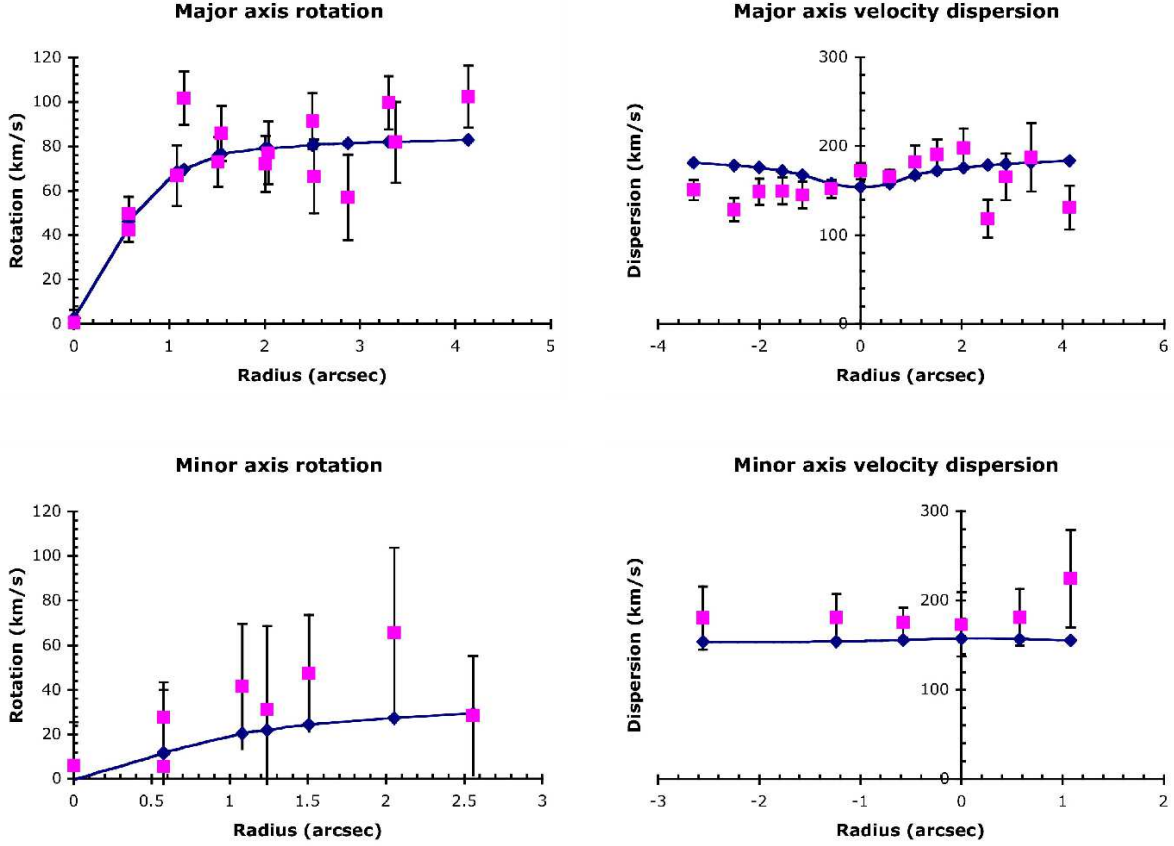


Figure 5. (Left) Major (upper) and minor (lower) axis data (pink squares) and fits (blue diamonds) for the rotation curve (inclined and calculated over an aperture) for the best-fitting solution. The measurement uncertainties on the data are also shown as error bars. (Right) Major (upper) and minor (lower) axis model and data line-of-sight velocity dispersion profiles for the best-fitting solution.

() display an anti-correlation, as do σ_h and scale length (r_h). Although these correlations do exist, the small error bars on the bulge convergence tightly constrain the overall model. We note that there is freedom in the halo model, but this is to be expected given that there are no independent constraints on its shape. This freedom in the halo model is reflected in the relatively large error bars quoted on its parameters. By marginalizing over remaining parameters, the error bars include the effects of these correlations between parameters.

The model fits to the kinematics are also of interest. Figure 5 shows the fits to the inner regions. The major axis kinematics are well recovered, within the observational errors, but the minor axis dispersion and rotation appear to be systematically low. It is possible that the omission of the bar in the central kinematics has contributed to this discrepancy.

Figure 6 displays the critical lines and caustic for the best-fitting model. The swallow-tail caustic feature and consequent non-elliptical critical line are due to the highly elliptical bar component. Note that the source does not lie close to the swallow-tail caustic and thus the details of the bar component do not strongly affect the image positions and magnifications.

Overall, the best-fitting model reproduces the data well

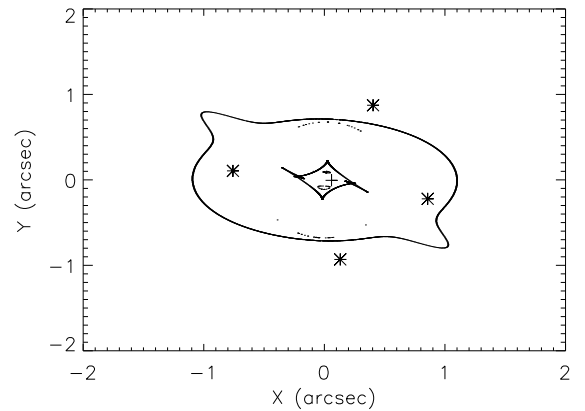


Figure 6. Critical lines and caustic for the best-fitting model. Also shown are the image positions (asterisks) and source position (plus). Note that both radial and tangential caustics are displayed.

considering the coarseness of the data and models. The kinematics are reproduced well with a kinematic best χ^2 of 76 for 44 kinematic data points (with 7 parameters to be fitted, giving 37 degrees of freedom). The lensing re-

Component	Mass enclosed $10^8 M$
Halb	8.8 ± 2.6
Bulge	142.5 ± 7.0
Disc	4.1 ± 1.0
Bar	11.6 ± 1.9

Table 4. Mass enclosed within the Einstein radius ($0.88''$) for each of the four mass components.

duced χ^2 is somewhat higher than unity, as expected because in general simple smooth models are not expected to reproduce the image configuration with astrometric precision. However, this level of precision is more than sufficient to determine robustly the total enclosed mass within the Einstein radius (Kochanek 1991; Treu & Koopmans 2004), the physical quantity that we are mostly interested in for our model. The mass within the Einstein radius ($0.88''$) is $(1.67 \pm 0.07) \times 10^{10} h_{70} M$, consistent with previous measurements (Wambsganss & Paczynski 1994; van de Ven et al. 2008). The components of this enclosed mass are described in Table 4. The components of the χ^2 are as follows: the lens image positions contribute 21.0% (representing 14.8% of the constraints), the H I points contribute 3.0% (3.7%), the inner rotation contributes 20.6% (42.6%), and the inner dispersion contributes 55.4% (38.9%).

4.1 Disc maximality and global parameters

With the best fitting model in hand we can now try to address the question of whether the stellar disc of the lens galaxy 2237+0305 is maximal or not. The relevant quantity for comparison with other observations and theory is $V_{2:2}=V_{\text{tot}}$, i.e. the ratio between the disc rotation velocity and the total rotation velocity measured at 2.2 scale lengths, close to the peak of the disc rotation curve. Based on the best fitting model, and taking into account the errors on the best fitting parameters, we find that $V_{2:2}=V_{\text{tot}} = 45 \pm 11\%$, consistent with a sub-maximal disc. The best fitting model also allows us to derive the global properties of the galaxy. The virial mass of the dark matter halo (calculated in a radius with an average density of 200_{crit}) is $(2.0 \pm 0.6) \times 10^{12} M$ (concentration parameter, $c = r_{200}=r_h = 13:3$), the stellar mass is $(7.4 \pm 0.3) \times 10^{10} M$ for the bulge and $(7.6 \pm 1.9) \times 10^{10} M$ for the disc. As expected for this particular lensing configuration, the bulge component is very well constrained, but interesting results can be obtained on the disc as well. The stellar to total mass ratio is $7:0 \pm 2:3\%$ in good agreement with typical numbers for galaxies of comparable mass.

5 DISCUSSION AND COMPARISON WITH PREVIOUS WORK

The constraints used to model the galaxy in Trott & Webster (2002) were image positions and the two neutral hydrogen rotation points at large radius (and well away from the image positions). Given that no kinematic information was available in the central regions, the inferred velocity curve due to the four mass components was

assumed to be circular. This means that an acceptable fit to the data was attainable with the four smoothly modelled mass components because the constraints effectively lie at only two radii – $0.9''$ (images) and $30''$ (H I data). There were considerable degeneracies in the model at other radii (e.g. see Figure 2 from Trott & Webster 2004).

In the present analysis, the addition of kinematic data provides additional constraints out to a radius of $5''$ (4 kpc). As displayed in Figure 3, constraining information is available in the central $5''$ and at two outer points in the galaxy, leaving the models to fit the remainder of radii according to their input density profiles. The bulge is well-constrained because it contributes considerably to the mass within the inner $5''$. The mass-to-light ratios of this study are more tightly constrained than those of Trott & Webster (2002) – their 1σ uncertainties were calculated while holding the values of other parameters at their minimum, thereby underestimating the true uncertainties. The bulge mass-to-light ratio is consistent with previous measurements from early-type galaxies $M/L_B = 7.9 \pm 2.3$ ($\mu_B = 0.70$) (Gerhard et al. 2001; Treu & Koopmans 2004). Similarly, Jiang & Kochanek (2007) report $M/L_B = 7.2 \pm 0.5$ ($\mu_B = 0.70$) from an analysis of 22 lens galaxies. As far as the disc mass-to-light ratio is concerned, our best fitting value is also consistent with typical measurements reported in the literature (e.g. Courteau & Rix 1999, and references therein).

The dark matter halo, however, contributes most to the outer regions of the galaxy where few constraints are available. In addition, unlike the bulge and disc, the absence of a light profile to guide the density profile of the dark matter yields additional freedom in the model. This allows a more flexible model, but also increases degeneracy. It is thus remarkable to see how well the dark matter halo is constrained by the available data. However, more detailed information about the structure of the dark matter halo would require information at radii greater than $6''$, where its influence increases. Alternatively, to gain more information about the halo from these data, one could place a prior on the bulge and disc mass-to-light ratios based on studies of other galaxies (or on stellar synthesis models) and determine whether such constraints narrowed the allowed value of the inner slope. This is left for future work.

The best-fitting solution described in Trott & Webster (2002) had a more massive disc and less massive halo compared with the best-fitting solution described here. The bulge mass was consistent between the two studies, within quoted errors. The errors quoted in Trott & Webster (2002) were calculated assuming no parameter covariances, and therefore underestimate the true errors as calculated by marginalising over the remaining parameters (as performed in this work). Therefore it is difficult to determine whether the halo and disc masses (and therefore the disc mass-to-light ratio) are consistent between the two studies. Note, however, that the dark matter halo mass profile used in this study was different to that in Trott & Webster (2002), allowing freedom in the inner slope.

The fit to the image positions in this study is not as good as the fit in Trott & Webster (2002). This is due to the increased complexity of the model in this work, and the need for the fit to balance the image positions and the kinematics. In Trott & Webster (2002), the image positions formed the most precise portion of the data (the H I points, being far

from the galactic centre and with relatively large error bars are easier to fit), and therefore were able to be well-fitted. In this work, the first and second order kinematics formed a relatively larger proportion of the χ^2 calculation, and therefore were fitted at the expense of the image positions.

In future work the modelling could be improved to include any effects of external shear (G2237+0305 has other less massive systems identified along the line-of-sight) and to include the kinematic effects of the bar more consistently. The former could improve the lensing component of the χ^2 without affecting the dynamical fit. In addition, the dark matter halo could be modelled to be non-spherical with flattening aligned with that of the disc (as suggested by studies of other lensing systems).

Despite the comparatively good model presented in this present work, it is important to keep in mind the following caveats. The lens galaxy 2237+0305 has additional structure that is not accounted for in the four component model, e.g. prominent spiral arms that are attached to the bar component. In addition, the bar is not treated in a self-consistent manner. These may not be important for the lensing but still produce anisotropy in the kinematics. The bar is difficult to model kinematically and an attempt has not been made in this work. However, in the central few arcseconds its presence is small and we opted to neglect it for the inner kinematics, including its effect only in the lensing and for the overall rotation curve.

The image magnifications and total magnification are dependent on the balance between the steepness and the anisotropy of the overall mass model. As demonstrated by Wambsganss & Paczynski (1994), 2237+0305 allows a range of models with degeneracy between the density slope and ellipticity. Inclusion of kinematics in our model has reduced that degeneracy. The magnification ratios are consistent with the mid-IR measurements of Agol et al. (2000). They argued that mid-IR measurements are the least likely to be contaminated by stellar microlensing, electron scattering and extinction (see also Chiba et al. 2005; Agol & Kochanek 2006).

In terms of global properties, the central galaxy is bulge-dominated, and modelling the mass distribution of the bulge accurately is most important for an accurate overall model. Beyond $r = 20''$, the halo appears to continue to increase in rotational support in the outer regions, and to absorb the rotation beyond the optical radius.

Our results can be compared with those of van de Ven et al. (2008). Their measured central velocity dispersion ($166 \pm 2 \text{ km s}^{-1}$) is consistent with that presented in this work ($172 \pm 9 \text{ km s}^{-1}$) within the errors. Although they had the advantage of two-dimensional data and the additional information that accompanies that, our data are based on stellar kinematics from the Mgb-Fe region, observed in a cleaner region of the sky than the CaII triplet targeted by their observations. This allowed us to reach further out in projected distance from the centre, albeit along preferred directions. The results of van de Ven et al. (2008) are complementary to ours: they fit a fourier-based lens model, fitting the image positions and flux ratios, and combine the information with the implied mass distribution from the kinematics and light distribution, to obtain an estimate of the luminous mass-to-light ratio. A comparison of this value with that

obtained using a single stellar population model yields a maximum dark matter contribution within the Einstein radius of 20%, which is higher than our best fit value of 7% and our upper limit of 15% (3). In addition, their comparison of the lens-based mass model and the observed luminosity distribution indicates that mass follows light in the inner regions, and any halo contribution is relatively constant. Our analysis focuses on determining a simple yet comprehensive description of the galaxy over a broader range of scales. Although the results for the dark matter halo can be improved by more extended and precise kinematic data, we achieved our aim of determining the bulge and disc mass-to-light ratios with good precision, without the need to use stellar population synthesis models. Future studies with the addition of stellar population synthesis models will be very valuable.

The good agreement between our results and those of van de Ven et al. (2008) (based on largely independent datasets (except for the strong lensing) and methodologies) is encouraging: the combination of lensing and dynamics is a powerful tool to study spiral galaxies, not only elliptical galaxies. As larger samples of spiral lens galaxies are being discovered by the SLACS (Bolton et al. 2008) and other surveys (including many where the Einstein radius will be equal or larger than the scale length of the disc) the combination of lensing, kinematics, and stellar population synthesis models should enable substantial progress in our understanding of the structure of disc galaxies, and therefore their formation and evolution.

6 SUMMARY

Data from the ESI echelle instrument on the Keck II telescope were used to measure the major and minor axis kinematics of the spiral lens galaxy 2237+0305. The rotation and velocity dispersion profile in the central few arcseconds of 2237+0305 are combined with the lensed-image positions and the rotation curve beyond the optical disc (H I rotation points) to construct a structural and kinematic model of 2237+0305. Four components are used to constrain the mass distribution: a dark matter halo with variable inner logarithmic slope and scale length; a de Vaucouleurs bulge, modelled structurally with a flattening consistent with the light profile; an exponential disc, inclined at 60° ; a Ferrers bar, at a position angle 39° from the disc major axis. The inner galaxy kinematics were modelled with an axisymmetric two-integral model composed of the bulge, disc, and dark matter halo.

The best-fitting solution shows that the lens galaxy is bulge-dominated in the inner regions, with a massive stellar disc and dark matter halo that provide rotational support beyond the bulge. The bulge and disc B-band mass-to-light ratios ($M/L_b = 6.6 \pm 0.3$, $M/L_d = 1.2 \pm 0.3$) are consistent with typical values found for local galaxies. The bulge mass is very well constrained by the combination of lensing and dynamics. The disc mass is less well constrained because of residual degeneracies with the halo mass, although the best solutions indicate a sub-maximal disc, contributing $45 \pm 11\%$ of the support at 2.2 scale lengths. The inner logarithmic slope of the dark matter halo is consistent with a negative inner logarithmic slope of $\gamma = -1$, with a preferred

value of $\beta = 0.9 \pm 0.3$ (note that this may still be dependent on our use of an axisymmetric two-integral kinematic model).

This work illustrates the potential of lensing and dynamics to investigate the internal structure of spiral galaxies (see also van de Ven et al. 2008). The system Q 2237+ 0305 was the natural starting point for this kind of investigation due to the unusually low redshift of the lens galaxy. It is encouraging that such a complex galaxy, including a bar in the central regions, can be described with a relatively simple model described here over a wide range of scales. A partial limitation of this target, however, is that the multiple images are located at a particularly small physical scale (significantly smaller than the effective radius of the bulge and the exponential scale length of the disc) due once again to the unusually low redshift of the lens galaxy. This implies that the lensing geometry has relatively little leverage on the dark matter halo, compared to typical lenses at higher redshifts where the Einstein radius can be up to a few half-light radii, where the dark matter halo starts to be a substantial fraction of the total mass (e.g. Treu & Koopmans 2004). Current and future samples of disc lens galaxies are likely to be found at higher redshift, thus providing an opportunity to break the disc-halo degeneracy even further, as well as to investigate evolutionary trends.

ACKNOWLEDGMENTS

We wish to thank the anonymous referee for improving the manuscript with suggestions that clarify our methodology. C.M.T. acknowledges the support provided by the David Hay Memorial Fund during preparation of this manuscript. L.V.E.K. is supported (in part) through an NWO-VIDI program subsidy (project number 639.042.505). T.T. acknowledges support from the NSF through CAREER award NSF-0642621, by the Sloan Foundation through a Sloan Research Fellowship, and by the Packard Foundation through a Packard Fellowship. Support for HST archival program # 9960 was provided by NASA through a grant from the Space Telescope Science Institute, which is operated by the Association of Universities for Research in Astronomy, Inc., under NASA contract NAS 5-26555. We thank Aaron Dutton, Randall Wyth and Phil Marshall for many insightful conversations.

APPENDIX A: DATA REDUCTION

The ESI observations require some special preparation and calibration before they can be combined and used for kinematic analysis. The calibration process undertaken includes the following steps: bias subtraction, flat-fielding, rectification, cosmic-ray rejection and sky subtraction. These steps were performed by the package EASI2D, which is developed by David J. Sand and T. Treu (Sand et al. 2004) for easy extraction of echelle orders.

Given the lack of emission lines in the spectra of the old stellar population, strong absorption features need to be used in the kinematic analysis. The canonical region for stellar absorption kinematics in the optical is the Mg b-Fe complex around 5200 Å rest frame shown in Figure A1 which was used as our primary kinematic dataset. As an additional

test, we also fitted the Na d doublet at 5892 Å, which is generally considered less reliable because of possible interstellar absorption (Sparks et al. 1997).

In practice, the Gauss-Hermite Pixel Fitting Software developed by R. P. van der Marel (<http://www-int.stsci.edu/~marel/software/pixelfit.html>) is employed to determine the kinematic properties along both the major and minor axes. The template and galaxy spectra are prepared to have the same resolution, number of pixels and wavelength range. They are then compared using the iterative fitting method described in van der Marel (1994). The variable parameters used to find the best-fitting (lowest χ^2) solution are the order of the polynomial fit to the continuum and the spectral type used as the template. The rotation curves were found to be quite robust to parameter variations, while as expected the velocity dispersion profile requires more care in choosing the parameters. The region shown in Figure A1 was found to be a good compromise between using a large enough region and avoiding as much as possible the broad AGN features. A large number of tests were run to explore spectral ranges, masking areas and polynomial order for continuum fitting. Our error bars include all these sources of errors which dominate over the random errors.

The radius range is also extended beyond the region where the galaxy signal is obvious in order to include as much information as can be obtained from the data. The data are binned radially to $0.6''$ bins, in order for the points to be independent given the seeing. The outer points do not produce good fits beyond $r \sim 4''$, the galaxy signal is lost in the noise. The best-fitting stellar templates are from Giant stars with type G 9 III to K 5 III, consistent with the imaging results of Yee (1988) and produce statistically indistinguishable fits. Figure A1 displays an example fit. The stability and accuracy of the kinematic results are very good – all templates produce mutually consistent fits and the residuals appear consistent with noise.

The Na d region gave consistent rotation curves to the Mg b-Fe region, but systematically higher velocity dispersion profiles by 25%. Possible explanations of this difference (in addition to the effects of interstellar absorption) are contamination by quasar light and the diversity of possibly kinematically distinct stellar populations in the targeted regions. Although we feel that our choice of the Mg b-Fe region is justified, we repeated our analysis using the Na d-based stellar velocity dispersion profile and found our results to change only marginally. None of the conclusions of this paper is affected significantly by this choice.

The centre of the galaxy is difficult to locate from the data due to the significant contamination from the lensed quasars and the difficulties associated with image deconvolution. We therefore symmetrize the data to match the shape of the curve on both sides to find the kinematic centre. Once the centre is found, the rotation curves are symmetric within errors. The kinematic profiles obtained with the four best-fitting templates have been averaged to produce the final major axis results. The analysis of the minor axis data is similar to that performed for the major axis.

The central line-of-sight velocity dispersion is consistent within 1% uncertainties between the major and minor axis: $\sigma_{\text{c}} = 172 \pm 9 \text{ km s}^{-1}$, which compares well with the result of van de Ven et al. (2008) of $\sigma_{\text{c}} = 166 \pm 2 \text{ km s}^{-1}$. Our un-

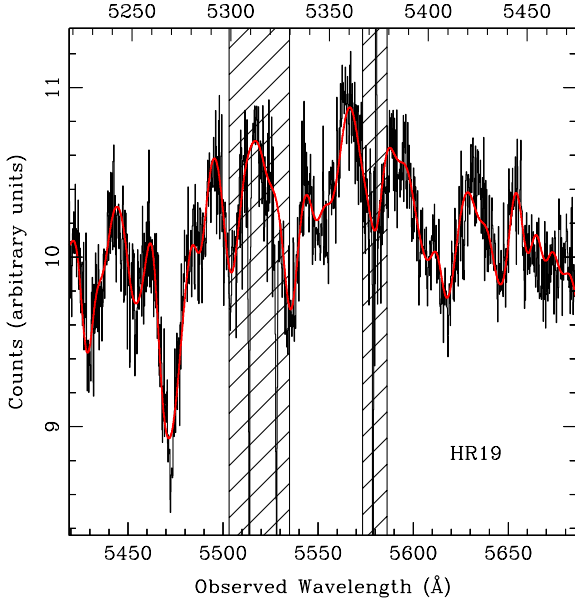


Figure A1. Best kinematic fit in the spectral region of the Mg and Fe absorption lines (rest wavelengths are indicated on the top axis of the plot). The data are shown as a black histogram, while the best fitting template is shown as a red curve. Spectral regions affected by intervening absorption line systems are masked out during the fit and shown as shaded areas.

certainties are larger, due to our inclusion of dominant systematic errors such as template and continuum mismatch. Our results are marginally lower than the value inferred by Foltz et al. (1992) ($215 \pm 30 \text{ km s}^{-1}$), possibly for the same reasons that cause the mismatch between the Mg b-Fe and Na d results.

APPENDIX B: TWO-INTEGRAL AXISYMMETRIC GALAXY MODELS

Here we briefly summarise the method of van der Marel & van Dokkum (2007) to produce axisymmetric dynamical models from photometric data. See the original paper for further details.

We assume the galaxy can be fitted with an axisymmetric model, and that there are two integrals of motion. In this regime, the two coupled Jean's equations are:

$$\frac{\partial}{\partial z} \frac{\overline{v_z^2}}{v_z^2} + \frac{\partial}{\partial z} \frac{h}{v_z^2} = 0; \quad (\text{B1})$$

$$\frac{\partial}{\partial R} \frac{\overline{v_R^2}}{v_R^2} + \frac{\partial}{\partial R} \frac{h}{R} + \frac{h}{R} \frac{\partial}{\partial R} \frac{1}{v_R^2} = 0; \quad (\text{B2})$$

where $\overline{v_R^2} = \overline{v_z^2}$.

The gradients of the gravitational potential, Φ , are calculated from the currently used mass density profiles of the mass components, according to (Binney & Tremaine 1987):

$$\Phi = -\frac{1}{r} = -G \sum_{i=1}^N \rho_i \frac{1}{r_i} \frac{Z}{r_i} \frac{1}{e_i^2 a_i} \frac{1}{(1 + \frac{r^2}{a_i^2})^{3/2}} \frac{1}{(1 + \frac{r^2}{b_i^2})^{3/2}} d; \quad (\text{B3})$$

where,

$$m^2 = a_i^2 = \frac{R^2}{1 + \frac{r^2}{a_i^2}} + \frac{z^2}{1 + \frac{r^2}{b_i^2}}; \quad (\text{B4})$$

and a_i, b_i are the semi-major and -minor axes of the mass component, and the summation is over all distinct mass components.

The mean streaming motion is not constrained by the Jean's equations, and van der Marel & van Dokkum (2007) introduce a constrained scaling parameter, k , to control the amount of rotation,

$$\overline{v} = k \frac{\overline{v^2}}{\overline{v_R^2}}; \quad (\text{B5})$$

The value of k is constrained by the necessity of positive dispersion everywhere,

$$k \geq \min_{(R,z)} \left[\overline{v^2} = (\overline{v^2} - \overline{v_R^2})^{1/2} \right]; \quad (\text{B6})$$

The mass components and velocity moments then need to be inclined to the viewing angle, and the projected line-of-sight moments determined according to,

$$\overline{h_w^m}(\mathbf{x}; \mathbf{y}) = \frac{1}{(\mathbf{x}; \mathbf{y})} \int_{-1}^1 (\mathbf{x}; \mathbf{y}; w) \overline{h_w^m}(\mathbf{x}; \mathbf{y}; w) dw; \quad (\text{B7})$$

where w denotes the line-of-sight direction, and,

$$\overline{v_w} = \overline{v} \cos i; \quad (\text{B8})$$

$$\overline{v_w^2} = (\overline{v^2} - \overline{v_R^2}) \cos^2 i + \overline{v_R^2}$$

are the first and second moments, and i is the inclination angle. The rotation component, V , and velocity dispersion, σ , are then derived as,

$$V = \langle \overline{v_w} \rangle; \quad (\text{B9})$$

$$\sigma^2 = V^2 + \overline{v_w^2} - V^2 = V^2 + \langle \overline{v_w^2} \rangle; \quad (\text{B10})$$

The prescription to determine the first and second velocity moments using this method is as follows:

For a given mass model, calculate the gravitational potential derivatives and density profiles on a (R, z) grid;

Calculate $\overline{v_z^2} = \overline{v_R^2}$ on the same grid according to B2;

Calculate \overline{v} on the same grid according to B2;

Calculate the mean streaming motion on the same grid, according to B5, and ensure it meets the positivity requirement;

Incline the density distributions of the mass components to the line-of-sight;

Calculate the line-of-sight first and second velocity moments;

Convolve the moments with seeing, slit width and pixel size.

REFERENCES

- Agol E., Jones B., Blaes O., 2000, ApJ, 545, 657
- Agol E., Kochanek C., 2006, in Bulletin of the American Astronomical Society Vol. 38 of Bulletin of the American Astronomical Society, Mid Infrared Observations of Quasar Lenses. pp 928{+}
- Bertin G., Ciotti L., Del Principe M., 2002, A & A, 386, 149
- Binney J., Tremaine S., 1987, Galactic Dynamics. Princeton, NJ, Princeton University Press

- Bolton A. S., Burles S., Koopmans L. V. E., Treu T., Gavazzi R., Moustakas L. A., Wayth R., Schlegel D. J., 2008, *ApJ*, 682, 964
- Bolton A. S., Treu T., Koopmans L. V. E., Gavazzi R., Moustakas L. A., Burles S., Schlegel D. J., Wayth R., 2008, *ApJ*, 684, 248
- Borriello A., Salucci P., 2001, *MNRAS*, 323, 285
- Bradac M., Clowe D., Gonzalez A. H., Marshall P., Forman W., Jones C., Markevitch M., Randall S., Schrabback T., Zaritsky D., 2006, *ApJ*, 652, 937
- Bucholz H., 1969, *The confluent hypergeometric function: with special emphasis on its applications*. Springer-Verlag
- Chiba M., Minezaki T., Kashikawa N., Katata H., Inoue K. T., 2005, *ApJ*, 627, 53
- Courteau S., Rich H., 1999, *ApJ*, 513, 561
- Crane P., Albrecht R., Barbieri C., et al. 1991, *ApJL*, 369, L59
- Czoske O., Bamabe M., Koopmans L. V. E., Treu T., Bolton A. S., 2008, *MNRAS*, 384, 987
- de Blok W. J. G., 2005, *ApJ*, 634, 227
- de Blok W. J. G., McGaugh S. S., Rubin V. C., 2001, *AJ*, 122, 2396
- Dutton A. A., Courteau S., de Jong R., Carignan C., 2005, *ApJ*, 619, 218
- Dutton A. A., van den Bosch F. C., Dekel A., Courteau S., 2007, *ApJ*, 654, 27
- Eigenbrod A., Courbin F., Sluse D., Meylan G., Agol E., 2008a, in *Proceedings of the Manchester Microlensing Conference: The 12th International Conference and AN-GLES Microlensing Workshop. Microlensing variability in the gravitationally lensed quasar Q 2237+0305 = Einstein Cross*
- Eigenbrod A., Courbin F., Sluse D., Meylan G., Agol E., 2008b, *A & A*, 480, 647
- Foltz C. B., Hewett P. C., Webster R. L., Lewis G. F., 1992, 386, L43
- Gerhard O., Kronawitter A., Saglia R. P., Bender R., 2001, *AJ*, 121, 1936
- Gilmer R., Lewis G. F., 2005, *A & A*, 437, L15
- Gorenstein M. V., Shapiro I. I., Falco E. E., 1988, *ApJ*, 327, 693
- Grieco C., Lombardi M., Rosati P., Bertin G., Gobat R., Demarco R., Lidman C., Motta V., Nonino M., 2008, *A & A*, 486, 45
- Halkola A., Seitz S., Pannella M., 2006, *MNRAS*, 372, 1425
- Hasan H., Burrows C. J., 1995, *PASP*, 107, 289
- Hayashi E., Navarro J. F., Power C., Jenkins A., Frenk C. S., White S. D. M., Springel V., Stadel J., Quinn T. R., 2004, *MNRAS*, 355, 794
- Huchra J., Gorenstein M., Kent S., Shapiro I., Smith G., Horne E., Perley R., 1985, *AJ*, 90, 691
- Jiang G., Kochanek C. S., 2007, *ApJ*, 671, 1568
- Keeton C. R., 2001, *astro-ph/0102341*
- Kent S. M., Falco E. E., 1988, *AJ*, 96, 1570
- Kochanek C. S., 1991, *ApJ*, 373, 354
- Koopmans L. V. E., de Bruyn A. G., Jackson N., 1998, *MNRAS*, 295, 534
- Koopmans L. V. E., Treu T., 2002, 568, L5
- Koopmans L. V. E., Treu T., 2003, *ApJ*, 583, 606
- Koopmans L. V. E., Treu T., Bolton A. S., Burles S., Moustakas L. A., 2006, *ApJ*, 649, 599
- Lewis G. F., Irwin M. J., Hewett P. C., Foltz C. B., 1998, *MNRAS*, 295, 573
- Lin Neto G. B., Gerbal D., Marquez I., 1999, *MNRAS*, 309, 481
- Linoulin M., Richard J., Jullo E., Kneib J.-P., Fort B., Soucail G., Elasdottir A., Natarajan P., Ellis R. S., Smail I., Czoske O., Smith G. P., Hudelot P., Bardeau S., Ebeling H., Egami E., Knudsen K. K., 2007, *ApJ*, 668, 643
- Lokas E. L., Mamon G. A., Prada F., 2005, *MNRAS*, 363, 918
- Maller A. H., Simard L., Guhathakurta P., Hjorth J., Jaunsen A. O., Flores R. A., Primack J. R., 2000, *ApJ*, 533, 194
- Mihov B. M., 2001, *A & A*, 370, 43
- Moller O., Hewett P., Blain A. W., 2003, *MNRAS*, 345, 1
- Moore B., Quinn T., Governato F., Stadel J., Lake G., 1999, *MNRAS*, 310, 1147
- Muroz J. A., Kochanek C. S., Keeton C. R., 2001, *ApJ*, 558, 657
- Navarro J. F., Frenk C. S., White S. D. M., 1996, *ApJ*, 462
- Navarro J. F., Hayashi E., Power C., Jenkins A. R., Frenk C. S., White S. D. M., Springel V., Stadel J., Quinn T. R., 2004, *MNRAS*, 349, 1039
- Noordemeer E., 2008, *MNRAS*, 385, 1359
- Peng C. Y., Ho L. C., Impey C. D., Rich H. W., 2002, *AJ*, 124, 266
- Perez I., Fux R., Freeman K., 2004, *A & A*, 424, 799
- Rauch M., Sargent W. L. W., Barlow T. A., Simcoe R. A., 2002, *ApJ*, 576, 45
- Sackett P. D., 1997, *ApJ*, 483, 103
- Sand D. J., Treu T., Smith G. P., Ellis R. S., 2004, *ApJ*, 604, 88
- Schmidt R. W., 1996, *Masters Thesis*, pp 2(+
- Schneider D. P., Turner E. L., Gunn J. E., Hewitt J. N., Schmidt M., Lawrence C. R., 1988, *AJ*, 96, 1755
- Sersic J. L., 1968, *Atlas de galaxias australes*. Cordoba, Argentina: Observatorio Astronomico
- Shin E. M., Evans N. W., 2007, *MNRAS*, 374, 1427
- Sparks W. B., Carollo C. M., Maccchetto F., 1997, *ApJ*, 486, 253
- Treu T., Koopmans L. V. E., 2004, *ApJ*, 611, 739
- Trott C. M., Webster R. L., 2002, *MNRAS*, 334, 621
- Trott C. M., Webster R. L., 2004, in *IAU Symposium 220 Determining the Properties of Galaxy 2237+0305 using Gravitational Lensing*. pp 109(+
- Udalski A., Szymanski M., Kubiak M., Pietrzynski G., Soszynski I., Zebrun K., Szczyk O., Wyrzykowski L., Ulaczyk K., Wiercinski T., 2006, *Acta Astronomica*, 56, 293
- Vakulik V. G., Schild R. E., Smailov G. V., Dudinov V. N., Tsvetkova V. S., 2007, *MNRAS*, 382, 819
- van Albada T. S., Sancisi R., 1986, *Royal Society of London Philosophical Transactions Series A*, 320, 447
- van de Ven G., Falcon-Barroso J., McDermid R. M., Cappellari M., Miller B. W., de Zeeuw P. T., 2008, *astro-ph/0807.4175*
- van der Marel R. P., 1994, *MNRAS*, 270, 271
- van der Marel R. P., van Dokkum P. G., 2007, *ApJ*, 668, 738
- Verheijen M. A. W., Bershady M. A., Swaters R. A., Andersen D. R., Westfall K. B., 2007, in *Island Universes - Structure and Evolution of Disk Galaxies Astrophysics*

- and Space Science Proceedings, The Disk Mass Project:
breaking the disk-halo degeneracy. pp 95{100
- Wambsganss J., Paczynski B., 1994, *AJ*, 108, 1156
- Wayth R. B., O'Dowd M., Webster R. L., 2005, *MNRAS*,
359, 561
- Windhorst R. A., Burstein D., Mathis D. F., Neuschaefer
L. W., Bertola F., Buson L. M., Koop D. C., Matthews K.,
Barthel P. D., Chambers K. C., 1991, *ApJ*, 380, 362
- Winn J. N., Hall P. B., Schechter P. L., 2003, *ApJ*, 597,
672
- Wozniak P. R., Alard C., Udalski A., Szymanski M., Ku-
biak M., Pietrzynski G., Zebrun K., 2000, *ApJ*, 529, 88
- Wucknitz O., 2002, *MNRAS*, 332, 951
- Yee H. K. C., 1988, *AJ*, 95, 1331
- Yoo J., Kochanek C. S., Falco E. E., McLeod B. A., 2006,
ApJ, 642, 22
- Zackrisson E., Bergvall N., Marquart T., Ostlin G., 2006,
A & A, 452, 857
- Zhao H., 1996, *MNRAS*, 278, 488